UNIVERSIDADE DE SÃO PAULO

INSTITUTO DE FÍSICA
CAIXA POSTAL 20516
01000 - SÃO PAULO - SP
BRASIL

publicações

IFUSP/P-419

THE ^{130}Te(p,p') REACTION ON ANALOG RESONANCES

M.C.H.M. Ruiz and M.L. Cescato
Instituto de Física, Universidade de São Paulo

J.L. Foster Jr.
Dept. of Physics, University of Notre Dame, Notre Dame, Indiana 46556 and
Intermetrics, Inc., Warminster, PA 18974

and

F. Krmpotić
Instituto de Física, Universidade de São Paulo
and
Departamento de Física, Facultad de Ciencias Exactas, Universidad Nacional de La Plata, 1900 La Plata, Argentina

Julho/1983

THE ^{130}Te(p,p') REACTION ON ANALOG RESONANCES

M.C.H.M. Ruiz and M.L. Cescato

Instituto de Física, Universidade de São Paulo
São Paulo, Brasil

J. L. Foster Jr.

Dept. of Physics, University of Notre Dame,
Notre Dame, Indiana 46556 and
Intermetrics, Inc., Warminster, PA 18974
and
F. Krmpotić*

Instituto de Física, Universidade de São Paulo
São Paulo, Brasil

and

Departamento de Física, Facultad de Ciencias Exactas,
Universidad Nacional de La Plata, 1900 La Plata, Argentina

Angular distributions for elastic and inelastic scattering have been measured on six analog resonances in the ^{130}Te + p system and at two off resonance energies. Partial widths are deduced from the angular distributions. Formulae for the spectroscopic amplitudes within the framework of quasiparticle random phase approximation are presented. The experimental results are compared with the theoretical predictions.

NUCLEAR REACTIONS ^{130}Te(p,p') E = 7.5 - 14 MeV; enriched targets; measured $\sigma(E_p,\theta)$; deduced spectroscopic amplitudes; ^{131}Te calculated and spectroscopic amplitudes predicted.

*Permanent address: Departamento de Física, Facultad de Ciencias Exactas, Universidad Nacional de La Plata, 1900 La Plata, Argentina. Fellow of the Consejo Nacional de Investigaciones Científicas y Técnicas de Argentina.

INTRODUCTION

The study of the elastic and inelastic proton scattering on analog resonances provides an important source of nuclear sreucture information related to the question of parentage[1-7]. That is, from these processes we can learn to what extent a nuclear state can be built up by adding a nucleon in a definite single-particle state to a definite core state. More precisely, the inelastic scattering gives a direct measure of:

i) the particle-vibrator coupling in the parent nucleus of the decaying proton is above the neutron Fermi level, and

ii) the microscopic structure of the core states, when the proton decays from a level which is below the neutron Fermi level.

In a recent paper[7] we have analysed the elastic and inelastic decays of the isobaric analog resonances in ^{144}Sm + p system associated with the low lying states of the parent nucleus ^{145}Sm with spin and parity $J^{\pi}_{\nu} = 7/2^-_1$, $3/2^-_1$, $1/2^-_1$. All the single-particle orbitals ($f_{1/2}$, $p_{3/2}$, $p_{1/2}$ and $f_{5/2}$) which, togheter with the positive parity vibrational fields establish the structure of these states, lie above the neutron Fermi level. Therefore, the main information which can be obtained from that study is related to the particle-vibrator coupling; the microscopic structure of the core plays only a minor role.

In the present work we study proton inelastic scattering to the ^{130}Te 2^+_1 state through analog resonances $3/2^+_1$, $1/2^+_1$, $7/2^-_1$, $3/2^-_1$, $3/2^-_2$ and $1/2^-_1$ in ^{131}I. In this case the negative parity states are also built up dominantly from the single-particle states, which are above the neutron Fermi level. The positive

parity resonances on the contrary comes from the orbitals which lie below or just on the top of the neutron Fermi surface. As a consequence, for the $3/2^+_1$ and $1/2^+_1$ resonances, both the particle-vibrator coupling in the parent nucleus and the macroscopic structure of the vibrational 2^+_1 field turn out to be relevant.

In the same way as in Ref. 7 we make use of the coupled channel formulation for treating the direct non-resonant scattering. However, as a) the analog resonances under study lie 7 to 10 MeV above the neutron threshold where there is a vast phase space available for neutron decay of the $T^<$ states and b) proton decay of the $T^<$ states is inhibited by the Coulomb barrier, the fluctuation contribution to be proton cross-section should be nil. Thus, contrarily to what happens in the ^{144}Sm + p system, the proton scattering in this work can be well described by considering a direct background amplitude and a resonant amplitude due to the presence of the analog states.

The fluctuation processes, as well as the different estimates for the single-particle escape amplitudes, have been thoroughly discussed in Ref. 7. Here the main emphasis is put on the nuclear structure calculation of the parentage coefficients.

It should be noted that previous measurements[8-11] on ^{130}Te lacked forward angle data and the analysis did not include the non-resonant direct mechanism.

II. EXPERIMENT

With the proton beam of the São Paulo Pelletron-8UD accelerator angular distribution of $\sigma(\theta)$ were measured between

40^o and 169^o at laboratory energies of 8.00, 8.30, 10.29, 10.54, 10.60 and 11.00 MeV. These energies are at or near those of analog resonances having J^π of $3/2^+$, $1/2^+$, $7/2^-$, $(3/2^-)$, $3/2^-$ and $(1/2^-)$ respectively, and correspond to maximum yield in the first 2^+ state averaged over several angles. Off-resonance angular distributions were taken at 7.50 MeV, 9.90 MeV and 14.00 MeV at angles between 30^o and 170^o. An array of three surface barrier detectors was used, each subtending a solid angle of about 1 msr. The detectors were cooled to 0^oC using a water-ice mixture.

Targets were made by vacuum evaporation of 99.4% enriched ^{130}Te from a gold plated Ta crucible onto 10μgm/cm² carbon foils and were about 200μgm/cm² in thickness. The carbon foils were evaporated onto clean $BaCl_2$ coated micro - scope slides by electron bombardment of graphite. Commercial foils and those prepared with a detergent substrate had contaminants which hindered the experiment. Targets made by evaporation from unplated crucibles contained tantalum teluride and were not stable in the beam.

Absolute cross-sections, accurate to within 5%, were determined by normalization of forward angle elastic scattering data to optical model predictions. The error bars on the data points are purely statistical and do not contain this error.

III. ANALYSIS

The method of analysis is identical to that of Ref. 7. Following Ref. 12 we express the cross section in terms of the C matrix defined by

$$C(cc'J)=C^{B}(cc'J)-\frac{i}{2}\frac{k_{c'}}{k_c}\left(\frac{2\ell+1}{2\ell'+1}\right)^{1/2}e^{-2i\sigma_{c'}}S^{R}(cc'J), \quad (3.1)$$

where J is the angular momentum of the resonance; $c\equiv\{n\ell jI\}$ and $c'\equiv\{n'\ell'j'I'\}$ stand, respectively, for the entrance and exit channel quantum numbers; k_c and σ_c are the wave number and Coulomb phase. The background term $C^{B}(cc'J)$ is calculated using the program coupled channel JUPITOR[12]. The spectroscopic information is contained in the resonant part of the scattering matrix, which reads in the R matrix formalism[13]

$$S^{R}(cc'J)=ie^{i(\phi_c+\phi_{c'})}\sum_{\nu}\frac{g(cJ_\nu)g(c'J_\nu)}{E_{J_\nu}-E-\frac{i}{2}\Gamma_J^T}, \quad (3.2)$$

with

$$\phi_c=\xi_c+\sigma_c+\psi_c^R. \quad (3.3)$$

Here, E the is incident center of mass energy, E_{J_ν} the resonance energy of the ν-th state with spin J, Γ_J^T the total width of the resonance, ξ_c the real optical phase and ψ_c^R the resonance mixing phase. The resonance amplitudes $g(cJ_\nu)$ are related to the spectroscopic amplitudes $\theta(cJ_\nu)$ through the expression[14,15]

$$\theta(cJ_\nu)=\left[\frac{2T_o+1}{2P_c^o}\right]^{\frac{1}{2}}\frac{g(cJ_\nu)}{\gamma_c^{s.p.}} \quad (3.4)$$

where T_o denotes the isospin of the target nucleus, P_c^o the optical-model penetrability and ζ_c the imaginary part of the optical phase. The quantity $\gamma_c^{s.p.}$ is the single particle reduced width given by

$$\gamma_c^{s.p.}=\left(\frac{\hbar^2}{2ma_c}\right)^{\frac{1}{2}}\mu_n^2(a_c) \quad (3.5)$$

where $\mu_n(a_c)$ is the value of the neutron wave function at the channel radius a_c and m is the neutron mass. The minimun values of $\left[(2T_o+1)/2P_c^o\right]^{1/2}/\gamma_c^{s.p.}$ in the region of the nuclear surface were calculated by program ANSPEC[14,15] and used in the determination of the $\theta(cJ_\nu)$. The spectroscopic factor is simply given as $S(cJ_\nu)=\theta^2(cJ_\nu)$.

The coupled channel optical potential was obtained by fitting elastic and inelastic angular distributions at 7.5 and 14.0 MeV using program ECIS[16] which solves the coupled equations by a method of sequential iterations. The first 2^+ state is considered as a one phonon vibration. Fig. 1 shows the fits and the optical parameters. The deformation parameter β_C was taken from the Coulomb excitation[17] B(E2), 0.295 e^2b^2, using the relation

$$B(E\lambda)=\left(\frac{3}{4\pi}Ze\beta_C R_C^{\lambda}\right)^2,$$

where Z is the atomic number and R_C is the Coulomb radius. A linear dependence in energy was assumed for V and W, the real volumn and surface imaginary potential depths. Using the 7.5 and 14 MeV potentials one obtains

$V = -0.59E + 60.49$ MeV,

$W = 0.58E + 3.93$ MeV.

The 9.9 MeV elastic and inelastic angular distributions which are affected by the 10.29 MeV resonance showed a best fit indicating a dependence of about

$W = 0.48\ E + 5.37$ MeV.

This gave improved resonance fits, particularly at 8.038 MeV and was used throughout this work.

Resonance mixing phases and elastic partial widths come from a reanalysis of the 170° scattering excitation curves of Ref. 9 using program ANSPEC[14,15]. Fig. 2, shows fits to two resonance regions. We obtain $\psi^R_{\ell=0} = 9^o$, $\psi^R_{\ell=1} = 7^o$, $\psi^R_{\ell=2} = 5^o$, $\psi^R_{\ell=3} = 0^o$. These phases are then used in inelastic fitting. The "on-resonance" angular distributions were taken at the energies of the maximum yield of the first 2^+ which are not the resonance energies. The quantity $E_{J_\nu} - E$ was determined by varying E until the elastic angular distributions were fit. Fig. 3, shows the elastic resonant angular distributions.

The only free parameters in the inelastic analysis are the $g(cJ_\nu)$. Once the correct combination of signs for the $g(cJ_\nu)$ is found, the iteration procedure rapidly converges. The resonances were fitted separately, but every three iterations the background due to the other resonances was corrected. Table I, shows the deduced elastic and inelastic parameters. Errors are estimated from behavior during fitting and do not include the normalization uncertainly.

IV. CALCULATION

IV.1. Nuclear Model

We attempt to describe the energy spectra and the spectroscopic amplitudes in terms of the pairing-plus-

multipole model (PMM) with the quasiparticle random phase approximation (QRPA) for the doubly even system and the quasiparticle vibration coupling (QVC) for the odd-even system. A detailed description of the PMM model can be found in Ref. 18; here we shall merely sketch the main approximations involved in this model and derivate the formulae for the spectroscopic amplitudes, which are not available in the literature.

The PMM consists of the one-body shell model Hamiltonian (H_{sp}), with the short range pairing (H_p) and long range multipole (H_M) forces as a residual two-body interaction. Usually, the pairing coupling constant G is fixed from the experimental pairing energy Δ and the neutron-neutron, proton-proton and neutron-proton multipole forces are chosen to be equal:

$$\chi_\lambda^{nn} = \chi_\lambda^{pp} = \chi_\lambda^{nn} \equiv \chi_\lambda$$

The QRPA implies:

i) An approximate diagonalization of the Hamiltonian $H_{sp} + H_p$ through the Bogoljubov quasiparticle transformation

$$\alpha^+_{jm} = u_j a^+_{jm} + v_j a_{j\bar{m}}; \quad a_{j\bar{m}} = (-)^{j+m} a_{j-m}\ , \tag{4.1}$$

leading to the independent quasiparticle Hamiltonian

$$H_{qp} = \sum_{jm} E_j \alpha^+_{jm} \alpha_{jm}. \tag{4.2}$$

The operator $a^+_{jm}(a_{j\bar{m}})$ creates (annihilates) a particle in the state $|jm\rangle(|j,-m\rangle)$ and $j\equiv\{n\ell j\}$; the corresponding quasiparticle operators are, respectively, α^+_{jm} and $\alpha_{j\bar{m}}$. The symbol E_j

stands for the independent quasiparticle energy

$$E_j = \left[(\varepsilon_j - \varepsilon_F)^2 + \Delta^2\right]^{1/2}, \tag{4.3}$$

where ε_F is the Fermi energy, Δ is the energy gap and ε_j is the single particle energy.

The multipole operators

$$M^\mu_\lambda = \sum_{\substack{j_1 m_1 \\ j_2 m_2}} \langle j_1 m_1 | i^\lambda r^\lambda Y^\mu_\lambda | j_2 m_2 \rangle a^+_{j_1 m_1} a_{j_2 m_2} \ , \tag{4.4}$$

contained in H_M, become

$$M^\mu_\lambda = M^\mu_\lambda(s) + M^\mu_\lambda(p), \tag{4.5}$$

where

$$M^\mu_\lambda(s) = \sum_{j_1 j_2} S(j_1 j_2 \lambda) s^\mu_\lambda(j_1 j_2), \tag{4.5a}$$

$$M^\mu_\lambda(p) = \frac{1}{2} \sum_{j_1, j_2} P(j_1 j_2 \lambda) \left[p^{\mu\,+}_\lambda(j_1 j_2) + (-)^{\lambda-\mu} p^{-\mu}_\lambda(j_1 j_2)\right], \tag{4.5b}$$

with

$$S(j_1 j_2 \lambda) = (2\lambda+1)^{-\frac{1}{2}} \ (U_{j_1} U_{j_2} - V_{j_1} V_{j_2}) \langle j_1 || i^\lambda r^\lambda Y_\lambda || j_2 \rangle, \tag{4.6a}$$

$$P(j_1 j_2 \lambda) = (2\lambda+1)^{-\frac{1}{2}} \ (U_{j_1} V_{j_2} + U_{j_2} V_{j_1}) \langle j_1 || i^\lambda r^\lambda Y_\lambda || j_2 \rangle, \tag{4.6b}$$

$$s^\mu_\lambda(j_1 j_2) = \left[\alpha^+_{j_1} \alpha^+_{\tilde{j}_2}\right]^\mu_\lambda, \tag{4.6c}$$

$$p^{\mu\,+}_\lambda(j_1 j_2) = \left[\alpha^+_{j_1} \alpha^+_{j_2}\right]^\mu_\lambda. \tag{4.6d}$$

ii) The scattering terms in the multipole Hamiltonian are dropped out and the QRPA Hamiltonian

$$H_{QRPA} = H_{qp} - \frac{1}{2} \sum_{\lambda\mu} \chi_\lambda (-)^{\lambda-\mu} M^{-\mu}_\lambda(p) M^\mu_\lambda(p) \ , \tag{4.7}$$

is brought into the diagonal form:

$$H_{coll} = \sum_{\lambda\mu, i} \hbar\omega_{\lambda,i} \ B^{\mu+}_{\lambda,i} \ B^\mu_{\lambda,i} \ , \tag{4.8}$$

by the Bogoljubov transformation

$$B^{\mu+}_{\lambda,i} = \frac{1}{2} \sum_{j_1 j_2} \left[a_i(j_1 j_2 \lambda) p^{\mu+}_\lambda(j_1 j_2) - b_i(j_1 j_2 \lambda) (-)^{\lambda-\mu} p^{-\mu}_\lambda(j_1 j_2)\right] , \tag{4.9}$$

where

$$a_i(j_1 j_2 \lambda) = \Lambda_{\lambda,i} \frac{P(j_1 j_2 \lambda)}{E_{j_1} + E_{j_2} - \hbar\omega_{\lambda,i}} \ , \tag{4.10a}$$

$$b_i(j_1 j_2 \lambda) = \Lambda_{\lambda,i} \frac{P(j_1 j_2 \lambda)}{E_{j_1} + E_{j_2} + \hbar\omega_{\lambda,i}} \ , \tag{4.10b}$$

are, respectively the forward and backward going amplitudes with the normalization condition

$$\sum_{j_1 j_2} \left[a_i(j_1 j_2 \lambda) a_{i'}(j_1 j_2 \lambda) - b_i(j_1 j_2 \lambda) b_{i'}(j_1 j_2 \lambda)\right] = 2\delta_{ii'}. \tag{4.11}$$

The eigenfrequencies $\omega_{\lambda,i}$ are obtained form the dispersion relation

$$\chi_\lambda^{-1} = \frac{1}{2}\sum_{j_1 j_2}\left[P(j_1 j_2 \lambda)\right]^2\left[\frac{1}{E_{j_1}+E_{j_2}-\hbar\omega_{\lambda,i}} + \frac{1}{E_{j_1}+E_{j_2}+\hbar\omega_{\lambda,i}}\right] \tag{4.12}$$

while the quantity $\Lambda_{\lambda,i}$ is given by the expression

$$\Lambda_{\lambda,i}^{-2} = \frac{\partial}{\partial(\hbar\omega_{\lambda,i})}\left[\chi_\lambda^{-1}\right] = \frac{1}{2}\sum_{j_1 j_2}\left[P(j_1 j_2 \lambda)\right]^2\left[\frac{1}{(E_{j_1}+E_{j_2}+\hbar\omega_{\lambda,i})^2} - \right.$$

$$\left. - \frac{1}{(E_{j_1}+E_{j_2}-\hbar\omega_{\lambda,i})^2}\right] \tag{4.13}$$

After applying the inverse transformation to eq. (4.5b) the phonon multipole operator reads

$$M_\lambda^\mu = \chi_\lambda^{-1}\sum_i \Lambda_{\lambda,i}\left[B_{\lambda,i}^{\mu+} + (-)^{\lambda-\mu}B_{\lambda,i}^{-\mu}\right]. \tag{4.14}$$

For the odd system the Hamiltonian is written in the form

$$H_{odd} = H_{qp} + H_{coll} + H_{int}(QVC) \tag{4.15}$$

where

$$H_{int}(QVC) = \sum_{\lambda\mu,i}\Lambda_{\lambda,i}M_\lambda^{\mu+}(s)\left[B_{\lambda,i}^{\mu+} + (-)^{\lambda-\mu}B_{\lambda,i}^{-\mu}\right]. \tag{4.16}$$

The wave functions of the Hamiltonian (4.15) are expressed as a superposition of one quasi-particle, one quasi-particle plus one phonon, etc.:

$$|JM\rangle = |C_J\alpha_{JM}^+ + \sum_{j,i}C_{j\lambda,iJ}\sum_{m\mu}(jm\lambda\mu|JM)\alpha_{jm}^+B_{\lambda,i}^{\mu+} + \ldots|\psi_o\rangle \tag{4.17}$$

$$\equiv C_J|JOJM\rangle + \sum_{j,i}C_{j\lambda iJ}|j\lambda_i;JM\rangle + \ldots .$$

where $|\psi_o\rangle$ is the ground-state wave function of the even system (BCS-vacuum).

The actual calculation shows that only the lowest energy phonon, which corresponds to the vibrational state, is important. This is not only because its energy is the lowest, but also because it is strongly coupled to the single-quasi-particles ($\Lambda_{\lambda,1}$ is large). Therefore we will consider only the lowest phonon, drop the suffix i and use the number of phonons N, together with the total angular momentum I, to specify the many phonon system. The energy matrix element of the Hamiltonian H_{odd} is given by

$$\langle j'N'I'J|H_{odd}|jNIJ\rangle = \delta_{jj'}\delta_{NN'}\delta_{II'}(N\hbar\omega_\lambda + E_j)$$

$$-\Lambda_\lambda(-)^{\lambda+I'+J+j}(2\lambda+1)^{1/2}\begin{Bmatrix} j' & I' & J \\ I & j & \lambda\end{Bmatrix}S(j'j\lambda) \tag{4.18}$$

$$\times\left[\langle N'I'||B_\lambda^+||IN\rangle\delta_{N',N+1} + \langle N'I'||B_\lambda^{+H}||NI\rangle\delta_{N',N-1}\right],$$

where $B_{\lambda\mu}^{+H} = (-)^{\lambda-\mu}B_{\lambda-\mu}$. In particular

$$\langle j'N'=1,I'=\lambda,J=j|H_{odd}|j,N=0,I=0,J=j\rangle = -\Lambda_\lambda\left(\frac{2\lambda+1}{2j+1}\right)^{1/2}S(jj'\lambda) \tag{4.19}$$

It should be noted that the relation between the quantitly Λ_λ and the macroscopic particle-vibration coupling strength <k> is given by

$$\Lambda_\lambda = \frac{<k>}{<r^\lambda>} \frac{\beta_\lambda}{(2\lambda+1)^{1/2}} \tag{4.20}$$

where $<k>=<r\partial V/\partial r>\approx 50$MeV and $<r^\lambda>=3/(3+\lambda)R^\lambda$ with $R=1.2A^{1/3}$fm, A being the mass of the nucleus considered.

We are now ready to calculate the spectroscopic amplitudes defined by

$$\theta(jNIJ) = (2J+1)^{1/2} <IAS;J||a_j^{(p)+}||I> \tag{4.21}$$

and which measure to what extent the isobaric analog state (IAS) with the angular momentum J can be built up by adding a proton, in the single-particle state j, to a core state with N phonons and angular momentum I; T_o is the isospin of the target nucleus. The IAS is related with the low-lying parent state (PS) through the relation

$$|IAS;J> = \frac{T^-}{(2T_o+1)^{1/2}}|PS;J> \tag{4.22}$$

where $T^- = \sum_{jm} a^{p+}_{jm} a^n_{jm}$ is the isospin lowening operator. The final result is

$$\theta(jNIJ) = (-)^{I+j-J} C_{jNIJ} U_j^{(n)} U_j^{(p)} U_j^{(p)} + \sum_{j'N'I'} (-)^{I+I'+\lambda} (2\lambda+1) C_{j'N'I'J} \begin{Bmatrix} I & I' & \lambda \\ j' & j & J \end{Bmatrix}$$

$$\times \{[V_j^{(n)} U_j^{(p)} U_j^{(p)} b^{(n)}(j'j\lambda) + U_{j'}^{(n)} U_j^{(p)} V_{j'}^{(p)} b^{(p)}(j'j\lambda) + U_{j'}^{(n)} V_{j'}^{(p)} U_j^{(p)} a^{(p)}(j'j\lambda)]\delta_{N',N+1}$$

$$+[V_j^{(n)} U_j^{(p)} U_j^{(p)} a^{(n)}(j'j\lambda) + U_{j'}^{(n)} U_j^{(p)} V_j^{(p)} a^{(p)}(j'j\lambda) + U_{j'}^{(n)} V_{j'}^{(p)} U_j^{(p)} b^{(p)}(j'j\lambda)]\delta_{N',N-1}\} \tag{4.23}$$

To discuss the physical features of the spec - troscopic amplitudes, it is useful to give explicit formulae for specific cases. In the following, the cases which involve ground and the first vibrational state of an even nucleus are listed. Contributions from two phonon states in the odd nucleus are neglected. The cases are:

a) Even Nucleus in the Ground State (Elastic Scattering):

$$\theta(j,I=0,J=j) = C_j U_j^{(n)} U_j^{(p)} U_j^{(p)} - \left(\frac{2\lambda+1}{2j+1}\right)^{1/2} \sum_{j'} C_{j'\lambda j}$$

$$\times [V_j^{(n)} U_j^{(p)} U_j^{(p)} b^{(n)}(jj'\lambda) + U_{j'}^{(n)} U_j^{(p)} V_j^{(p)} b^{(p)}(jj'\lambda) + U_{j'}^{(n)} V_j^{(p)} U_j^{(p)} a^{(p)}(jj'\lambda)], \tag{4.24a}$$

b) Even Nucleus in the First Excited State (Inelastic Scattering):

$$\theta(j,I=\lambda,J) = (-)^{j-J+\lambda}\{C_{j\lambda J} U_j^{(n)} U_j^{(p)} U_j^{(p)} - \left(\frac{2\lambda+1}{2J+1}\right)^{1/2} C_J$$

$$\times [V_j^{(n)} U_j^{(p)} U_j^{(p)} a^{(n)}(Jj\lambda) + U_J^{(n)} U_J^{(p)} V_j^{(p)} a^{(p)}(Jj\lambda) + U_J^{(n)} V_J^{(p)} U_j^{(p)} b^{(p)}(Jj\lambda)]. \tag{4.24b}$$

The amplitudes C_J and $C_{j\lambda J}$ are obtained from the diagonalization of the Hamiltonian (4.16). This procedure, however, leaves hidden those physical processes which play

the dominant role in creating the properties of the coupled system. More over, the results of diagonalization sometimes show a certain asymptotic behaviour which could be eventually predicted without complicated numerical operations. For these reasons, the results for the spectroscopic amplitudes are listed below, when only zeroth and first order contributions to the wave functions are considered. This means that:

I) For a predominantly single-quasiparticle state the wave function of the parent state is approximated by:

$$|JM\rangle \approx |J0JM\rangle - \Lambda_\lambda \left(\frac{2\lambda+1}{2J+1}\right)^{\frac{1}{2}} \sum_{j'} \frac{S^{(n)}(Jj\lambda)}{E_J - \hbar\omega_\lambda - E_j} |j\lambda JM\rangle \qquad (4.25)$$

and

$$\theta(j,I=0,J=j) = U_j^{(n)} U_j^{(p)} U_j^{(p)} - \Lambda_\lambda^2 \left(\frac{2\lambda+1}{2j+1}\right) \sum_{j'} \frac{S^{(n)}(jj'\lambda)}{E_j - E_{j'} - \hbar\omega_\lambda}$$
$$\times \left[\frac{V_j^{(n)} U_j^{(p)} U_j^{(p)} P^{(n)}(jj'\lambda)}{E_j^{(n)} + E_{j'}^{(n)} + \hbar\omega_\lambda} + \frac{U_{j'}^{(n)} U_{j'}^{(p)} V_j^{(p)} P^{(p)}(jj'\lambda)}{E_j^{(p)} + E_{j'}^{(p)} + \hbar\omega_\lambda} + \frac{U_{j'}^{(n)} V_{j'}^{(p)} U_j^{(p)} P^{(p)}(jj'\lambda)}{E_j^{(p)} + E_{j'}^{(p)} - \hbar\omega_\lambda} \right] \qquad (4.26a)$$

in the case a) and

$$\theta(j,I=\lambda,J) = -\Lambda_\lambda \left(\frac{2\lambda+1}{2J+1}\right)^{\frac{1}{2}} \left[\frac{U_J^{(n)} U_j^{(n)} U_j^{(p)} S^{(n)}(jJ\lambda)}{E_J^{(n)} - E_j^{(n)} - \hbar\omega_\lambda} \right.$$
$$\left. + \frac{V_j^{(n)} U_j^{(p)} U_j^{(p)} P^{(n)}(jJ\lambda)}{E_j^{(n)} + E_j^{(n)} - \hbar\omega_\lambda} + \frac{U_J^{(n)} U_J^{(p)} V_j^{(p)} P^{(p)}(jJ\lambda)}{E_J^{(p)} + E_j^{(p)} - \hbar\omega_\lambda} + \frac{U_J^{(n)} V_J^{(p)} U_j^{(p)} P^{(p)}(jJ\lambda)}{E_J^{(p)} + E_j^{(p)} + \hbar\omega_\lambda} \right] \qquad (4.26b)$$

in the case b);

II) For a predominantly collective state the wave function is approximated by:

$$|JM\rangle \approx |j'\lambda JM\rangle - \Lambda_\lambda \left(\frac{2\lambda+1}{2J+1}\right)^{\frac{1}{2}} \frac{S^{(n)}(Jj'\lambda)}{E_{j'} + \hbar\omega_\lambda - E_J} |J0JM\rangle \qquad (4.2\ )$$

and

$$\theta(j,I=0,J=j) = -\Lambda_\lambda \left(\frac{2\lambda+1}{2j+1}\right)^{\frac{1}{2}} \left[\frac{U_j^{(n)} U_j^{(p)} U_j^{(p)} S^{(n)}(jj'\lambda)}{E_{j'} + \hbar\omega_\lambda - E_j} \right.$$
$$\left. + \frac{V_j^{(n)} U_j^{(p)} U_j^{(p)} P^{(n)}(jj'\lambda)}{E_j^{(n)} + E_{j'}^{(n)} + \hbar\omega_\lambda} + \frac{U_{j'}^{(n)} U_{j'}^{(p)} V_j^{(p)} P^{(p)}(jj'\lambda)}{E_j^{(p)} + E_{j'}^{(p)} + \hbar\omega_\lambda} + \frac{U_{j'}^{(n)} V_{j'}^{(p)} U_j^{(p)} P^{(p)}(jj'\lambda)}{E_j^{(p)} + E_{j'}^{(p)} - \hbar\omega_\lambda} \right] \qquad (4.26a')$$

in the case a), and

$$\theta(j,I=\lambda,J) = (-)^{j-J-\lambda} \{ U_j^{(n)} U_j^{(p)} U_j^{(p)} - \Lambda_\lambda^2 \left(\frac{2\lambda+1}{2J+1}\right) \frac{S^{(n)}(Jj'\lambda)}{E_{j'} + \hbar\omega_\lambda - E_J}$$
$$\times \left[\frac{V_j^{(n)} U_j^{(p)} U_j^{(p)} P^{(n)}(Jj\lambda)}{E_J^{(n)} + E_j^{(n)} - \hbar\omega_\lambda} + \frac{U_J^{(n)} U_J^{(p)} V_j^{(p)} P^{(p)}(Jj\lambda)}{E_J^{(p)} + E_j^{(p)} - \hbar\omega_\lambda} + \frac{U_J^{(n)} V_J^{(p)} U_j^{(p)} P^{(p)}(Jj\lambda)}{E_J^{(p)} + E_j^{(p)} + \hbar\omega_\lambda} \right] \qquad (4.26b')$$

in the case b). The graphical representation of different terms in Eqs. (4.26a), (4.26b), (4.26a') and (4.26b') is displayed in Figs. 4a., 4b., 4a', and 4b', respectively. From these figures it is easy to see the physical meaning of each one of the contributions to the spectroscopic amplitude. For example, the last term in Eq. (4.26b) (last diagram in Fig. 4b) arises from the ground state correlations in the parent state, which create a phonon and two quasiprotons; the proton in the state $J^{(p)}$ is annihilated, together with the initial quasineutron in the state $J^{(n)}$, by the operator T^-, while the second proton decays from the state $j^{(p)}$ leaving the nucleus in the first vibrational state.

The first terms which appear in Eqs. (4.26) correspond to the conventional processes in which one neutron above the Fermi level is transformed, by means of the T^- operator, into a proton which latter on decays. The first terms in Eqs. (4.25) include, in addition, all the possible processes in which one or more phonons are successively emitted and absorbed through the scattering vertices. The decay modes mentioned above are the only ones which can take place in the usual macroscopic QVC model. In this coupling scheme the quasiparticle and collective degrees of freedom are treated as if they were independent of each other, i.e. $[\alpha_{jm}, B^{\mu}_{\lambda}]=0$, and the vibrational field causes only the scattering of the quasiparticles, but neither creates nor destroys pairs of quasiparticles. The remaining three terms in each one of Eqs. (4.25) and (4.26) arise either when the

microscopic structure of the phonons is explicitely taken into account or, equivalently, when one allows, within the macroscopic QVC model for the pair creation and pair destruction processes, in the first order perturbation theory. In the present work we have followed the first option; in the second case one should substitute the operator $M^{\mu+}_{\lambda}(s)$ in Eq. (4.16) by the operator $M^{\mu+}_{\lambda}=M^{\mu+}_{\lambda}(s)+M^{\mu+}_{\lambda}(p)$ and impose the condition $[\alpha_{jm}, B^{\mu}_{\lambda}]=0$.

Both from the formulae (4.26) and the graphs shown in Fig. 4, it is easy to discover a close similarity between the cases Ia and IIb (by case Ia we mean the elastic scattering through a dominantely single-quasiparticle state, etc.). The parentage coefficient in both cases is mainly determined by the superconductive factor $U^{(n)}_j U^{(p)}_j U^{(p)}_j$, as the remaining three terms, being proportional to Λ^2_{λ}, are relatively small. More explicitely: the transitions from the multiplet $|j\lambda J=|j-\lambda|,..,j+\lambda>$ to the one-phonon state $|\lambda>$ are of the same order of magnitude as the transition from the single-quasiparticle state $|j>$ on which is based the multiplet, independently of the value of the angular momentum J.

The cases Ib and IIa also bear a close resemblance. All the contributions are of first order in the coupling constant Λ_{λ}; in addition, when $\hbar\omega_{\lambda}>2\Delta$, all the pair creation and pair destruction factors carry the same sign, while the scattering form may interfer constructively or destructively depending on the interplay of the sign of its energy denominator with the sign of its superconductive vertex factor. A carefull analysis of the individual terms in Eqs. (4.26b)

and (4.26a') might lead to several interesting selection and intensity rules, similar to those which govern the electro - magnetic processes in a coupled system (see for example Ref. 19).

IV.2. Numerical Calculations

Table 2 shows the single particle energies ε_j used in the calculation. These come from the works of Heyde et al.[20] and Szanto de Toledo et al.[21]. The process of calculation was as follows. First the gap equations were solved, both for neutrons and for protons, with the gap parameters

$$\Delta^n = 1.16 \text{ MeV and } \Delta^p = 0.846 \text{ MeV},$$

taken from the experimental odd-even mass differences[22]. The corresponding pairing strengths and the Fermi energies were, respectively,

$$G^n = 0.145 \text{ MeV and } G^p = 0.142 \text{ MeV}$$

and

$$\varepsilon_F^n = 3.57 \text{ MeV and } \varepsilon_F^p = -3.18 \text{ MeV}.$$

The resulting quasiparticle energies and the occupation coefficients, shown in Table 2, were then used to

calculate the quasiparticle-phonon coupling constants Λ_λ for the first excited 2^+ and 3^- states in ^{130}Te nucleus, by means of Eq. (4.13). In this step we have employed harmonic oscillator wave functions with the length parameter $b=1.0057A^{1/3}$fm, and the experimental values for the phonon energies, i.e.

$$\hbar\omega_2 = 0.839 \text{ MeV and } \hbar\omega_3 = 2.72 \text{ MeV}.$$

Next, with the calculated coupling constants

$$\Lambda_2 = 0.154 \text{ MeV fm}^{-2} \quad \text{and} \quad \Lambda_3 = 0.0158 \text{ MeV fm}^{-3},$$

we have evaluated the amplitudes $a(j_1j_2\lambda)$ and $b(j_1j_2\lambda)$ and have proceeded with the diagonalization of the Hamiltonian H_{odd} in the basis

$$|j,(N_2N_3)N,\ (I_2I_3)I;\ JM\rangle;\ N=N_2+N_3,\ \vec{I}=\vec{I}_2+\vec{I}_3.$$

Here, N_λ and $\vec{I}_\lambda$ stand, respectively, for the number and angular momentum of the λ-pole phonon. Futhermore, the neutron quasiparticle was allowed to stay in one of the orbitals: $1g_{7/2}$, $2d_{5/2}$, $3s_{1/2}$, $1h_{11/2}$, $2d_{3/2}$, $2f_{7/2}$, $1h_{9/2}$, $3p_{3/2}$, $3p_{1/2}$, $1i_{13/2}$ and $2f_{5/2}$ and all collective states up to three quadrupole phonons ($N_3\leq 2$)) and two octupole phonons ($N_3\leq 2$) were considered. Finally, with the amplitudes C_{jNIJ}, obtained from the diagonalization procedure, we have calculated the parentage coefficients $\theta(jNIJ)$ given by Eq. (4.23).

In order to analyse the sensitivity of the theo - retical results on the model parameters and with the idea of getting the best possible fit to the experiments, several other calculations were performed, beside the one just mentioned. This study has revealed that the agreement, between the theoretical and measured energy spectra of ^{131}Te nucleus, improves significantly only when the quasiparticle-phonon scattering vertex is weakned rather drasticaly. The results which will be discussed immediately correspond to a effective scattering coupling constant

$$\Lambda_\lambda^{eff} = \Lambda_\lambda/2.5.$$

Although the only convincing justification for a such a procedure lies on the agreement with the experimental data it is worth to note that:

i) When the above mentioned QRPA values for Λ_2 and Λ_3 are used in the relation (4.20), with $\beta_2 = 0.109$ and $\beta_3 \approx 0.050$, we obtain for the macroscopic particle-vibration coupling strength, respectively, $\langle k \rangle = 70$ MeV and $\langle k \rangle = 90$ MeV; both of these values are significantly larger than those used in the previous theoretical studies of the odd-mass nuclei in the $A \approx 130$ mass region[6,20,21,23,24] ($\langle k \rangle$ between 30 and 50 MeV).

ii) The QRPA treatment includes only one-phonon states (or two quasiparticle states) while in the diagonalization of the Hamiltonian H_{odd} we have included also two and

three phonon states which are build up mainly from four and six quasiparticles. It is a well known fact that the main effect the two and three phonons have on the low-lying states of the coupled system is to increase the particle-phonon strength. Consequently, the extension of the collective subspace should be compensated with a diminution of the particle-phonon coupling constant.

V. RESULTS AND DISCUSSION

Fig. 4 shows the calculated level scheme compared with the experimental (d,p) work of Jolly[25] and Graue et al[26]. Jolly's work at 14.8 MeV had poor energy resolution ($\sim$ 50 keV) while the work of Ref. 25 with 9 keV resolution at 7.5 MeV was essentially coulomb stripping with unreliable ℓ-values for weak states. Most levels, calculated and observed, with $S_{dp} < .01$ are omitted from the figure. There are large discrepancies between the two (d,p) experiments as to observed levels, spectroscopic factors and excitation energies. Still it is clear that while the level scheme and spectroscopic factors, which is the QVC model read[18]

$$S_j = |C_j U_j^{(n)} - \left(\frac{2\lambda+1}{2j'+1}\right)^{\frac{1}{2}} V_j^{(n)} \sum_{j'} C_{j'\lambda j}|^2,$$

are globally reproduced, there are serious differences which could not be resolved by any change of parameters within the framework of the model employed. For example, the calculated

$1/2_1^+$ state is too low in energy and has a spectroscopic factor low by a factor of two. Increasing the $3s_{1/2}$ single particle energy causes the state to rise but further reduces the spectroscopic factor.

The 2.28 MeV $7/2^-$ level and 2.58 MeV, $3/2^-$ level are well reproduced in spectroscopic factors but the calculated level corresponding to the 2.51 MeV state appears 150 keV low in energy. Increasing $\varepsilon_{p_{3/2}}$ results in splitting of the $|2f_{7/2}, 0^+; 7/2^->$ configuration spectroscopic strength among a number of states. The 2.51 MeV ($3/2^-$) level has no clearly identified counterpart among the calculated states and we take the lowest energy calculated $3/2^-$ level for comparison of wave functions. We identify the lowest calculated $1/2^-$ state as corresponding to the 3.00 MeV ($1/2^-$) state in ^{131}Te.

Tables III and IV show the spectroscopic amplitudes deduced from the experimental data together with those from the model calculation. Errors are estimated from the behaviour of the partial widths in relation to χ^2 during fitting. Uncertainties in single particle widths are not taken into account. Figs. 5 and 6 show the fits to the inelastic data together with the angular distributions predicted by the calculation. There is an uncertainty of perhaps 20% in the predicted cross sections because of uncertainties in single particle widths and resonance total widths.

The experimental and calculated spectroscopic amplitudes on the $3/2^+$ resonance are in excellent agreement in both magnitude and sign. For the $1/2^+$ resonance the calculated

elastic spectroscopic amplitude is a bit too small. A really serious discrepancy is found in the amplitude $\theta(d_{3/2}, 2^+; 1/2^+)$. The measured value for this quantity indicates that: either both the particle-phonon and the core contributions are small or that they interfere destructively with each other. Theoreticaly, both amplitudes are large and add coherently due to the fact that the factor

$$\frac{U^{(n)}_{s_{1/2}} U^{(n)}_{d_{3/2}} - V^{(n)}_{s_{1/2}} V^{(n)}_{d_{3/2}}}{E^{(n)}_{s_{1/2}} - E^{(n)}_{d_{3/2}} - \hbar\omega_2}$$

which appears in the first term of Eq. (4.26b) is positive. In order to invert this situation one of the conditions $(E^{(n)}_{s_{1/2}} - E^{(n)}_{d_{3/2}}) > \hbar\omega_2$ or $U^{(n)}_{s_{1/2}} U^{(n)}_{d_{3/2}} > V^{(n)}_{s_{1/2}} V^{(n)}_{d_{3/2}}$ should be fulfilled. However, we have not succeeded to do that with any reasonable model parametrization. The amplitude $\theta(d_{5/2}, 2^+, 1/2^+)$ is quite well reproduced by the calculation.

For the negative parity states the overall agreement between measured and calculated spectroscopic amplitudes is satisfactory; the most pronounced misfit appears in the 2.47 MeV $3/2^-$ level.

The theoretical differencial cross sections are shown together the experimental results in Figs. 6 and 7. Most of the calculated curves show shapes comparable to the experimental ones and in particular at forward angles. As was expected the largest difference appears for the $1/2^+$ resonance.

IV. SUMMARY

We have performed the analysis of elastic and inelastic angular distribution of protons from ^{130}Te on isobaric analogue resonances considering at the same time resonant scattering and nonresonant scattering described by a coupled channel matrix, and good fits were obtained. Furthermore, it was demonstrated that the QRPA, with a multipole multipole force plus pairing,explains most of observed scattering data. Keeping in view the simplicity of the force, the agreement between the experiment and the theory is surprisingly good, in particular, for the high lying resonances. The remaining discrepancies are probably due to correlations and excitations not included in the approach employed here.

ACKNOWLEDGMENT

One of us (F.K.) is pleased to acknowledge many extremely helpful discussions with A.F.R. de Toledo Piza.

REFERENCES

[1] N. Auerbach, J. Hufner, A.K. Kerman, and C.M. Shakin, Rev. Mod. Phys. 44, 48 (1972).

[2] R.H. Boyd, R. Arking, J.C. Lombardi, A.B. Robbins, S. Yoshida, D.C. Slater, H.T. King, and R. Avida, Nucl. Phys. A.228, 253 (1974).

[3] S. Davis, G. Glashausser, and G. Bissinger, Nucl. Phys. A270, 285 (1976).

[4] K. Heide, M. Waroquier, and H. Yincx, Phys. Reports 26C, 277 (1976).

[5] F. Soga, Y. Hashimoto, N. Takahashi, Y. Iwasaki, K. Sakurai, S. Kohmoto, and Y. Nagami, Nucl. Phys. A288 504 (1977)

[6] J.L.Foster, Jr., F. Krmpotić, and T.V. Ragland, Phys. Rev. 17C, 1602 (1978).

[7] M.L.Cescato, M.C.H.M. Ruiz, J.L. Foster, and F. Krmpotić, Phys. Rev. (preceding paper).

[8] H.R. Hiddleston, and P.J. Riley, Phys. Lett. 32B, 425 (1970)

[9] H.R. Hiddleston, C. Hollas, V. Mistry, and P.J. Rilley, Phys. Rev. C3, 905 (1971).

[10] J. Brude, E. Engier, A. Grinsburg, A.A. Jaffe, A. Marinov, and L. Birstein, Nucl. Phys. A141, 375 (1970).

[11] J.L. Foster Jr., P.J. Riley, and C.F. Moore, Phys. Rev. 175, 1498 (1968)

[12] T. Tamura, Rev. Mod. Phys. 37, 679 (1965).

[13] W.J. Thomson, in Nuclear Isospin, edited by J.D. Anderson, S.R. Bloom, J. Cerny, and W.W. True (Academic, N.Y., 1970).

[14] W.J. Thompson, J.L. Adams, and D. Robson, Phys. Rev. 173, 975 (1968).

[15] W.J.Thompson, J.L. Adams, Technical Report ANSPEC, Tandem Accelerator Laboratory, Florida State University, Tallassee (unpublished).

[16] J. Raynal, in Computing as a Language in Physics, IAEA, Vienna, 1972), p. 918.

[17] A. Bockish, and A.M. Keinfeld, Nucl. Phys. A261, 508 (1969).

[18] S. Yoshida, Nucl. Phys. 38, 380 (1962).

[19] V. Paar, in Heavy-Ion, High-spin states and Nclear Structure (IAEA, Vienna, 1975) Vol. II, p. 179.

[20] K. Heyde, W. Waroquier, and H. Vincx, Phys. Lett. 57B, 429 (1975).

[21] A. Szanto de Toledo, M.N. Rao, O. Sala, and F. Krmpotić, Phys. Rev. C15, 238 (1977).

[22] A.G. Wapstra and N.B. Gove, Nucl. Data Tables 9, 267 (1971).

[23] G. Vanden Berghe, and M. Waroquier, Nucl. Phys. A196 , 203 (1976).

[24] V. Paar, and B.K.S. Koene, Z. Phys. A279, 203 (1976).

[25] R.K. Jolly, Phys. Rev. 136B, 683 (1964).

[26] A. Grave, E. Jastad, J.R. Lien, P. Torvund, and W.H. Moore, Nucl. Phys. A103, 209 (1967).

FIGURE CAPTIONS:

Figure 1. Optical Model Fits. The form of the potential is

$$U(r) = V_C - V\, f(r, R_o, a_o) - i\, W \frac{d}{dr} f(r, R_i, a_i)$$

$$+ \vec{\sigma}\cdot\vec{\ell} \left(\frac{\hbar}{m_\pi c}\right) \frac{Vso}{r} \frac{d}{dr} f(r, R_{so} A^{1/3}, a_{so}) \text{ where}$$

$f(r, R, a)$ is the usual Woods-Saxon form and R_C is the uniform sphere charge radius. We find $R_o = 1.25\ A^{1/3}$ fm, $a_o = 0.703$ fm, $R_i = 1.27\ A^{1/3}$ fm, $a_i = 0.634$ fm, $V_{7.5} = 57.06$ MeV, $W_{7.5} = 8.30$ MeV, $V_{14} = 52.23$, MeV, $W_{14} = 12.09$ MeV and take $V_{so} = 6.2$ MeV, $R_{so} = 1.10\ A^{1/3}$ fm, $a_{so} = 7.50$ fm $R_C = 1.20\ A^{1/3}$ fm with $\beta_C R_C = \beta_\nu R_\nu = \beta_I R_I = 0.690$ fm and $\beta_{so} = 0$.

Figure 2. Fits to 170° elastic excitation functions over 5 resonances.

Figure 3. Resonant elastic angular distributions. The curves correspond to the final values of $E_{J_\nu} - E$.

Figure 4. Lowest order diagrams contributing to the proton scattering in an analog resonance. In the graphs (a) and (b) the parent state is a single quasiparticle state and in the graphs (a') and (b') it is a member of the quasiparticle-phonon multiplet.The graphs (a) and (a') and (b) and (b') correspond, respectively to elastic and inelastic scattering. The pertinent analitic expressions are given by Eqs. (4.26).

Figure 5. Comparison of experimental and calculated level schemes. Columns (a) and (b) show energies, spins and (d,p) spectroscopic factors of Jolly[25] and Graue et al.[26], respectively. Column (c) shows calculated energies, spectroscopic factors and spins of levels with $S_{dp} \gtrsim .01$ and column (d) show the largest wave function component for the calculated states.

Figure 6. Even parity states. Solid lines indicate fits to inelastic angular distributions. Dotted lines are angular distributions predicted by the calculation.

Figure 7. Odd parity states. Conventions same as for Fig. 6.

TABLE I. Elastic and Inelastic Widths

A. Odd Parity Resonances. The value of $\Gamma_{p_1}^{9/2}$ was taken to be zero and held fixed on the $7/2^-$ resonance.

J^π	$E_{J_\nu}^{cm}$ (MeV)	$E_{J_\nu} - E$ (keV)	Γ_T(keV)	Γ_{p_o}(keV)	$\Gamma_{p_1}^{1/2^-}$(keV)	$\Gamma_{p_1}^{3/2^-}$(keV)	$\Gamma_{p_1}^{5/2^-}$(keV)	$\Gamma_{p_1}^{7/2^-}$
$7/2^-$	10.21	+5	78.0	17.0 ± 1	. . . . .	3.88 ± 0.3	0.132 ± 0.3	2.35 ± 0.3
$3/2^-$	10.45	+14	60.0	5.00 ± 1	1.18 ± 0.2	0.265 ±0.2	0.860 ±0.2	2.03 ± 0.2
$3/2^-$	10.51	+30	80.0	13.8 ± 1	3.27 ±0.4	3.55 ± 0.4	0.117 ±0.4	4.97 ± 0.4
$1/2^-$	10.90	+25	103	18.9 ± 1	. . . . .	12.47 ± 1.5	6.05 ± 1.5	. . . . .

B. Even Parity Resonances. The value of $\Gamma_{p_1}^{7/2}$ was taken to be zero and held fixed on the $3/2^+$ resonance.

J^π	$E_{J_\nu}^{cm}$ (MeV)	$E_{J_\nu} - E$ (keV)	Γ_T(keV)	Γ_{p_o}(keV)	$\Gamma_{p_1}^{1/2^+}$(keV)	$\Gamma_{p_1}^{3/2^+}$(keV)	$\Gamma_{p_1}^{5/2^+}$(keV)
$3/2^+$	7.98	0	65.0	6.00 ± 0.5	3.47 ± 0.3	1.76 ±0.3	0.495 ± 0.3
$1/2^+$	8.28	0	60.0	11.0 ± 1	. . . . .	0.0437±0.2	2.26 ± 0.2

TABLE II. Single particle energies, quasiparticle energies and the occupation coefficients used in the calculation.

$n\ell j$	Protons ε_j	E_j	V_j	Neutrons ε_j	E_j	V_j
$2f_{5/2}$	7.06	10.27	0.041	9.30	5.85	0.100
$1i_{13/2}$	6.42	9.63	0.044	9.10	5.65	0.103
$3p_{1/2}$	8.89	12.10	0.035	8.75	5.31	0.110
$3p_{3/2}$	7.61	10.82	0.039	8.50	5.07	0.115
$1h_{9/2}$	4.04	7.27	0.058	8.50	5.07	0.115
$2f_{7/2}$	4.42	7.64	0.055	7.30	3.91	0.150
$2d_{3/2}$	-0.350	2.95	0.145	2.90	1.40	0.882
$1h_{11/2}$	-0.485	2.82	0.152	2.60	1.59	0.918
$3s_{1/2}$	0.000	3.28	0.130	2.40	1.74	0.934
$2d_{5/2}$	-1.90	1.52	0.291	1.10	2.85	0.978
$1g_{7/2}$	-2.35	1.17	0.395	0.00	3.89	0.989
$1g_{9/2}$	-6.83	3.45	0.992	-3.83	7.63	0.997
$2p_{1/2}$	-7.10	4.15	0.995	-4.55	8.34	0.998
$1f_{5/2}$	-8.50	5.62	0.997	-6.04	9.82	0.998
$2p_{3/2}$	-8.38	5.41	0.997	-5.83	9.61	0.998
$1f_{7/2}$	-11.6	8.58	0.999	-9.02	12.78	0.999

TABLE III Even parity states. Comparison between experimental and calculated energies for the parent states and between experimental spectroscopic amplitudes and those obtained from model calculations. Calculated particle vibrator spectroscopic amplitudes (first term in Eq. (4.23)), summed core amplitudes (second term in Eq. (4.23)), and total spectroscopic amplitudes shown separately. We abbreviate $\theta(j,IJ)$ as $\theta(jI)$.

	J^π_ν	E(MeV)	$\theta(j,0^+)$	$\theta(s1/2,2^+)$	$\theta(d3/2,2^+)$	$\theta(d5/2,2^+)$	$\theta(g7/2,2^+)$	$\sum\theta^2$
Exp.	$3/2^+_1$	0.00	0.47±0.02	-0.30±0.01	0.37±.08	$-0.17^{+0.05}_{-0.06}$	. . .	0.82
P-vib amp		0.00	0.47	-0.093	0.14	-0.02	0.03	0.25
Th Core amp			. . .	-0.32	0.40	-0.13	0.19	
Total			0.47	-0.41	0.54	-0.15	0.24	0.75
Exp.	$1/2^+_1$	0.31	0.39±0.02	. .	$-0.05^{+0.07}_{-0.05}$	0.31±0.01	. . .	0.25
P-vib amp		0.11	0.28		0.24	0.06		0.14
Th Core amp		. . .	. . .		0.35	-0.22	. . .	
Total			0.28		0.59	0.28		0.51

TABLE IV Odd Parity States. Comparison between experimental and calculated energies for the parent states and between experimental spectroscopic amplitudes and those obtained from model calculations. Core amplitudes are negligible except for the $h11/2$ orbital which has $\theta_{core} = -0.10$ on the $7/2^-$ resonance.

	J^π_ν	E(MeV)	$\theta(j,0^+)$	$\theta(p1/2,2^+)$	$\theta(p3/2,2^+)$	$\theta(f5/2,2^+)$	$\theta(f7/2,2^+)$	$\theta(h9/2,2^+)$	$\theta(h11/2,2^+)$	$\sum\theta^2_{pv}$
Exp.	$7/2^-_1$	2.23	$0.76\pm.02$	. . .	$-0.33\pm.0.01$	$-0.09^{+0.08}_{-0.01}$	-0.35 ± 0.02	. . .	. . .	0.82
Theory		2.22	0.67	. . .	-0.23	-0.04	-0.40	0.04	-0.10	0.67
Exp.	$3/2^-_1$	2.47	0.32 ± 0.03	-0.18 ± 0.02	$-0.03^{+0.05}_{-0.09}$	-0.23 ± 0.03	-0.31 ± 0.02	. . .	. . .	0.28
Theory		1.90	0.11	-0.03	-0.04	-0.14	-0.20	. . .	. . .	0.08
Exp.	$3/2^-_2$	2.53	0.53 ± 0.01	-0.30 ± 0.02	-0.30 ± 0.02	$-0.08^{+0.09}_{-0.05}$	-0.47 ± 0.02	. . .	. . .	0.69
Theory		2.33	0.50	-0.15	-0.26	-0.08	-0.53	. . .	. . .	0.63
Exp.	$1/2^-_1$	2.92	0.63 ± 0.02	. . .	0.53 ± 0.03	-0.54 ± 0.07	. . .	. . .	. . .	0.96
Theory		2.68	0.40	. . .	0.52	-0.21	. . .	. . .	. . .	0.47

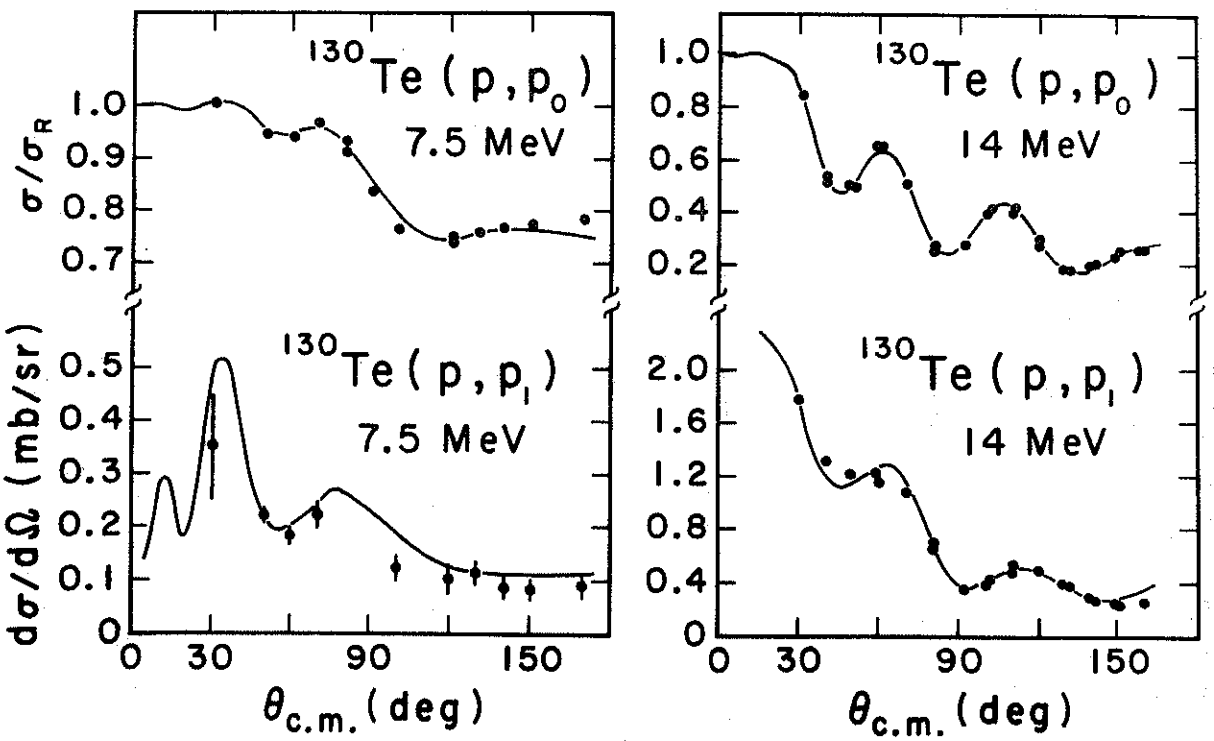

FIG. 1

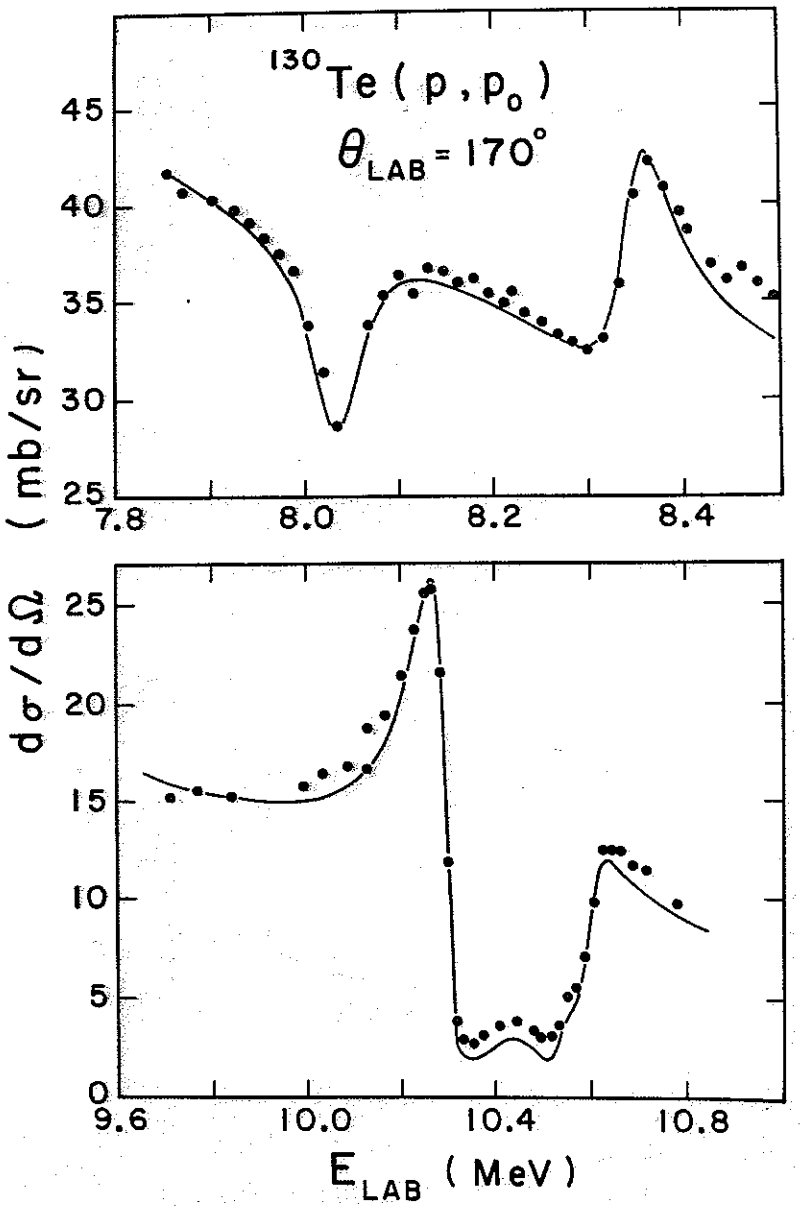
^{130}Te (p , p_0)
θ_{LAB} = 170°
dσ/dΩ (mb/sr)
E_{LAB} (MeV)

FIG. 2

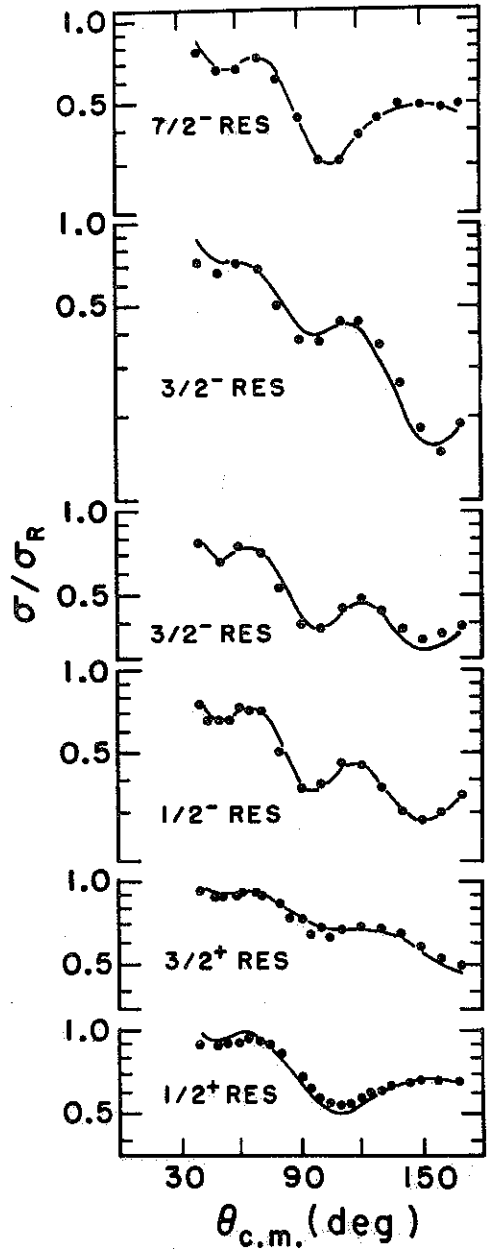
7/2⁻ RES
3/2⁻ RES
3/2⁻ RES
1/2⁻ RES
3/2⁺ RES
1/2⁺ RES
σ/σR
θc.m.(deg)

FIG. 3

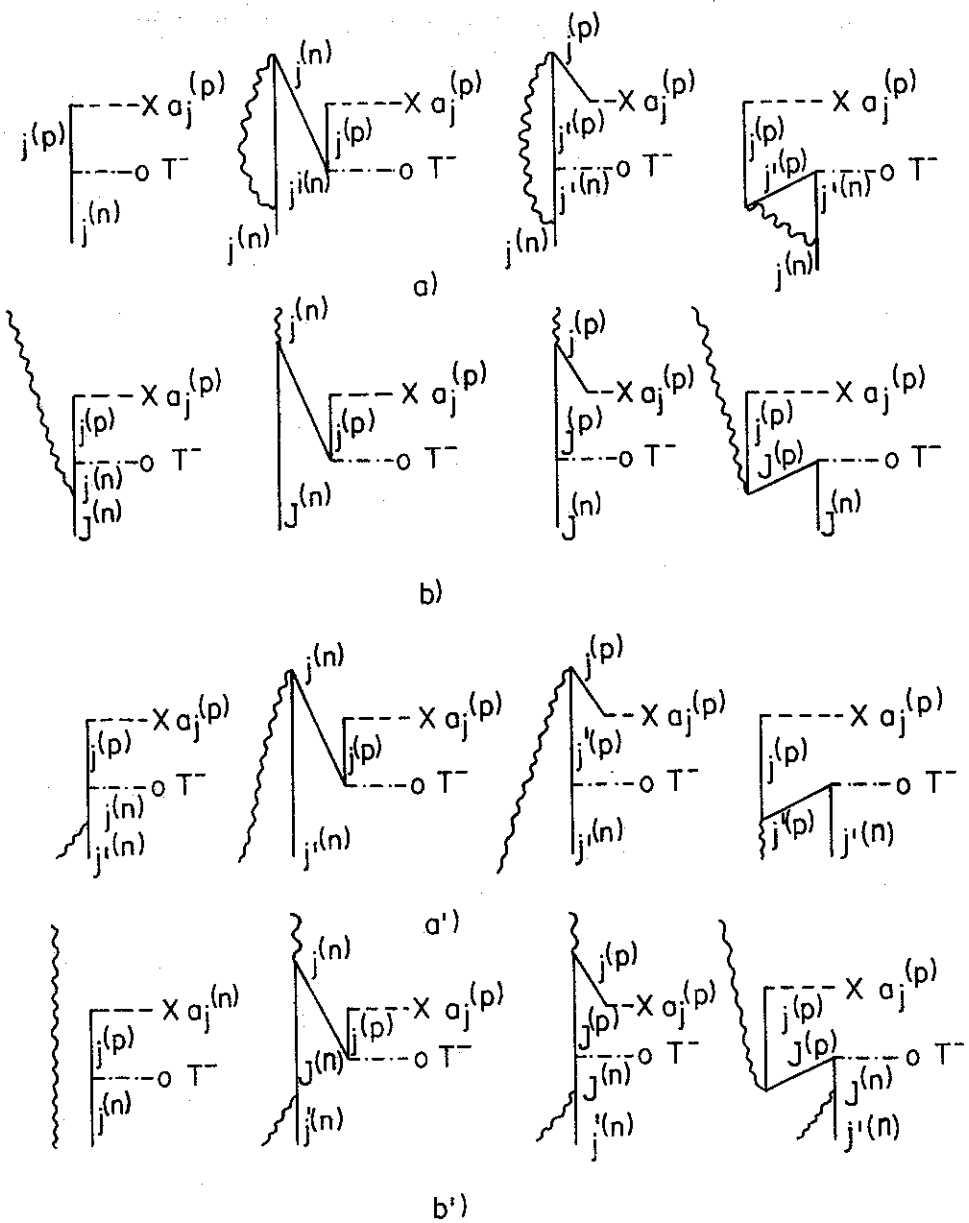
a)
b)
a')
b')

FIG. 4

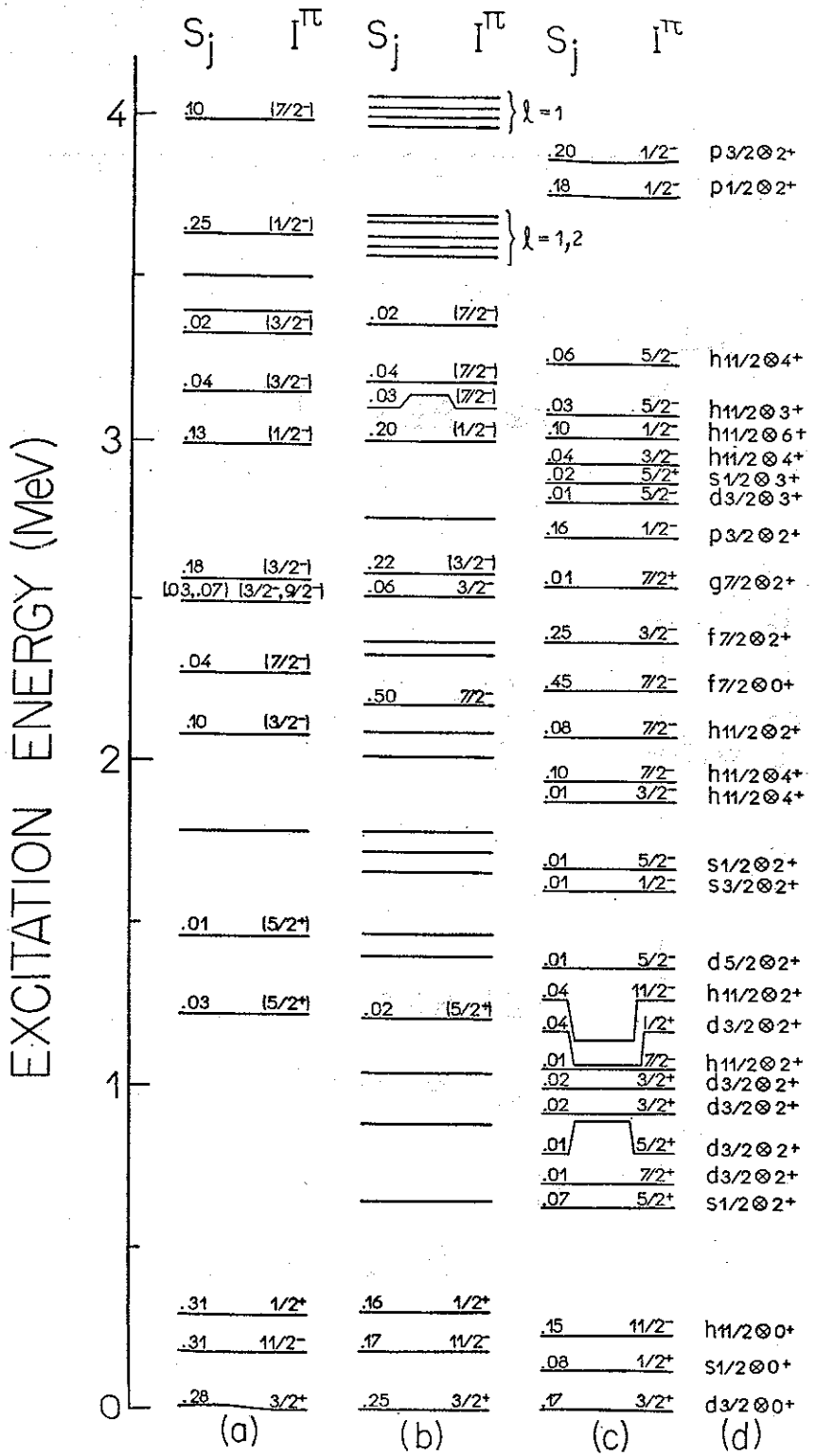
EXCITATION ENERGY (MeV)
Sj
Iπ
(a)
(b)
(c)
(d)
l = 1
l = 1,2
p3/2⊗2+
p1/2⊗2+
h11/2⊗4+
h11/2⊗3+
h11/2⊗6+
h11/2⊗4+
s1/2⊗3+
d3/2⊗3+
p3/2⊗2+
g7/2⊗2+
f7/2⊗2+
f7/2⊗0+
h11/2⊗2+
h11/2⊗4+
h11/2⊗4+
s1/2⊗2+
s3/2⊗2+
d5/2⊗2+
h11/2⊗2+
d3/2⊗2+
h11/2⊗2+
d3/2⊗2+
d3/2⊗2+
d3/2⊗2+
d3/2⊗2+
s1/2⊗2+
h11/2⊗0+
s1/2⊗0+
d3/2⊗0+

FIG. 5

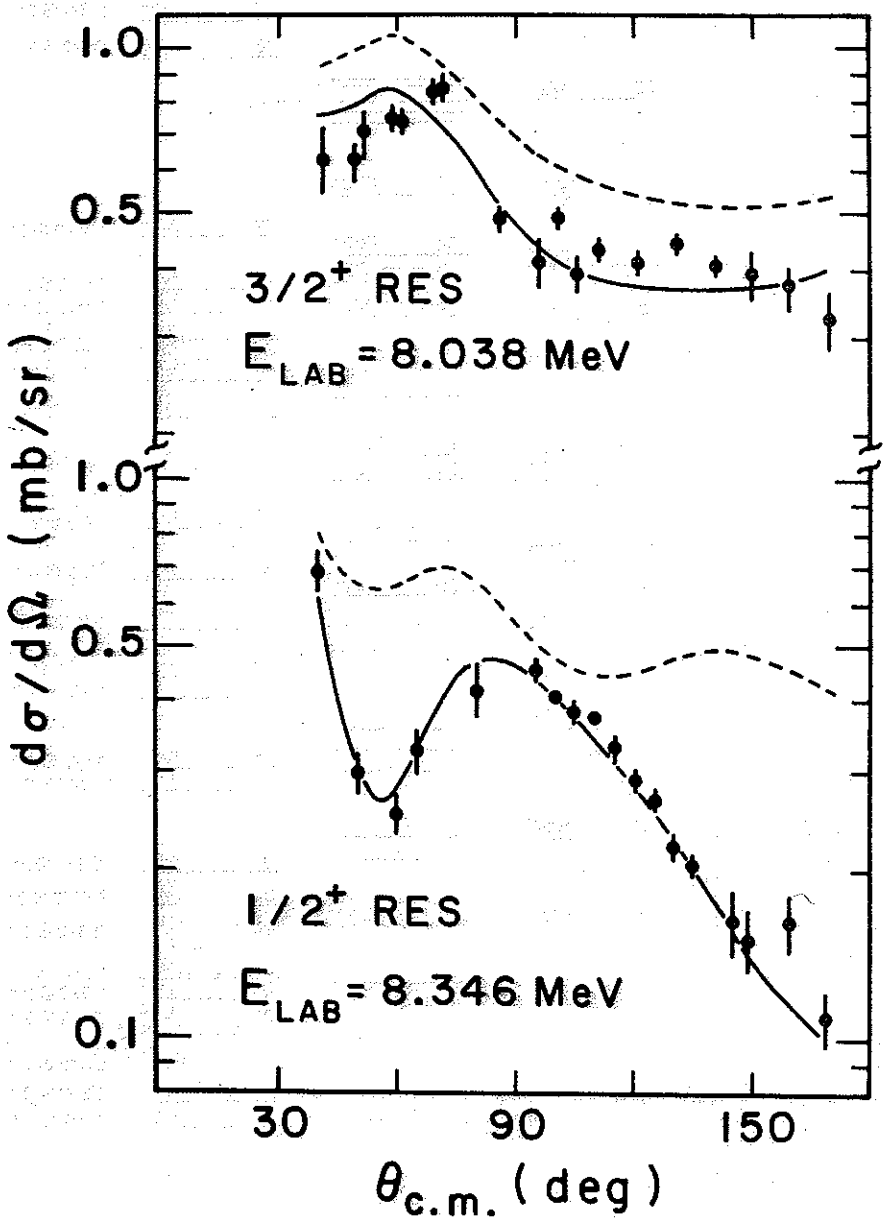
1.0
0.5
1.0
0.5
0.1
3/2+ RES
E_LAB = 8.038 MeV
1/2+ RES
E_LAB = 8.346 MeV
dσ/dΩ (mb/sr)
30
90
150
θc.m. (deg)

FIG. 6

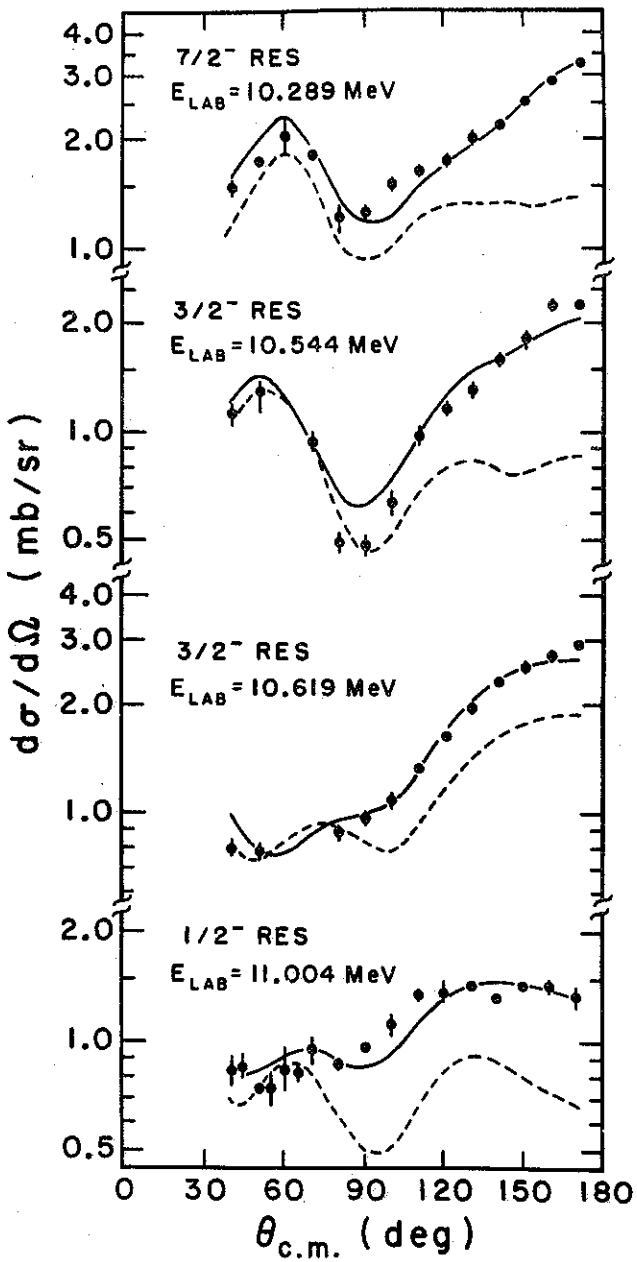
4.0
3.0
2.0
1.0
7/2- RES
E_LAB = 10.289 MeV
2.0
1.0
0.5
3/2- RES
E_LAB = 10.544 MeV
4.0
3.0
2.0
1.0
3/2- RES
E_LAB = 10.619 MeV
2.0
1.0
0.5
1/2- RES
E_LAB = 11.004 MeV
dσ/dΩ (mb/sr)
0
30
60
90
120
150
180
θc.m. (deg)

FIG. 7